Tellus (1988), *40B*, 437–445

Measurement of tropospheric OH concentrations by laser long-path absorption spectroscopy

By H.-P. DORN, J. CALLIES, U. PLATT and D. H. EHHALT, *Kernforschungsanlage Jülich GmbH, Institut für Chemie 3, Atmosphärische Chemie, Postfach 1913, D-5170 Jülich, FRG*

(Manuscript received 21 December 1987; in final form 17 March 1988)

ABSTRACT

Tropospheric hydroxyl (OH) radical concentrations were measured in summer 1987 in Jülich by broadband laser long-path absorption (laser-LPA) spectroscopy observing the $Q_1(2)$, $Q_{21}(2)$, $Q_1(3)$, $Q_{21}(3)$, and $P_1(1)$ rotational absorption lines around 308 nm. The measurement technique was improved using a multichannel spectrometric detector to record the OH absorption spectra. Now a much wider spectral interval can be observed at high resolution; thus, registration and correction of overlapping absorption features of interfering trace gases is improved. Simultaneous to the OH measurements, the concentrations of nitrogen dioxide (NO_2), formaldehyde (HCHO), and sulfur dioxide (SO_2) were monitored by a second LPA spectrometer. Ozone (O_3), aerosol concentrations, meteorological parameters, and absolutely calibrated photolysis frequencies of O_3 and NO_2 were also recorded. Carbon monoxide (CO), methane (CH_4), and light hydrocarbons were determined by gas chromatographic analysis. OH concentrations ranged up to $6.8 \cdot 10^6$ molecules/cm^3. At one day in July, an 'asymmetric' diurnal profile of the OH concentration was observed, which could be qualitatively explained by a strong decrease in the NO_2 concentration during the morning hours.

1. Introduction

Hydroxyl radicals play a central rôle in tropospheric chemistry. They determine atmospheric lifetime and concentration of a variety of trace gases. For example, oxidation of carbon monoxide, methane, alkanes, and isoprene in the atmosphere is initiated to more than ninety percent by the reaction with OH radicals (Ehhalt, 1974; Ehhalt, 1987; Volz et al., 1981; Zimmermann et al., 1978).

As a consequence of the high reactivity, the tropospheric OH concentration is very low, with noontime peak values rarely exceeding 10^7 molecules/cm^3. The measurement of OH radicals in the ambient atmosphere, therefore, makes high demands on the detection methods. An overview of earlier attempts to measure tropospheric OH is given, for instance, by Hewitt and Harrison (1985) and Hübler et al. (1984). Since then, a number of further experimental results have been published (Campbell et al., 1986; Hard et al., 1986; Davis et al., 1987; Shirinzadeh et al., 1987; Perner et al., 1987; Platt et al., 1987).

Because the reactions of OH radicals are very fast, the steady state OH concentration is established within minutes (Perner et al., 1987). Thus, OH chemistry takes place on a *local* scale. Its transport can be neglected. Due to the sensitivity of the OH concentration to changing trace gas concentrations, OH measurements are ideally suited for testing and improving zero-dimensional time dependent photochemical reaction models (*box models*) of the troposphere. Meaningful comparison of calculated and measured hydroxyl radical concentration is, however, only possible, if the parameters that determine the actual OH concentration in ambient air, are measured simultaneously to OH.

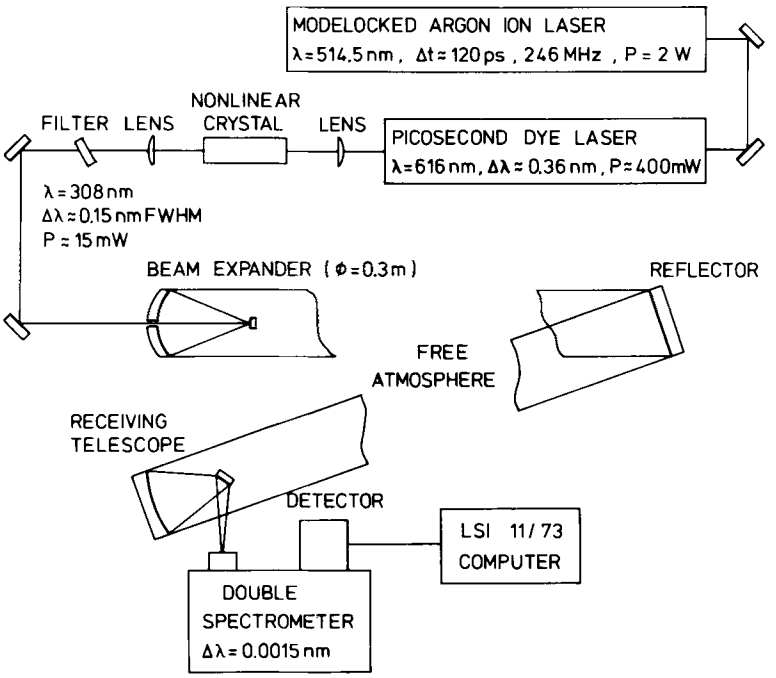

Fig. 1. Experimental setup for the OH radical detection by laser long-path absorption spectroscopy. The light path length in Jülich was 5.8 km.

2. Experimental

2.1. The OH-spectrometer

The tropospheric OH radical concentration was measured by laser long-path absorption spectroscopy. With the exception of the spectrometric detector, we essentially used the same setup as already described by Hübler et al., (1984). Hübler applied an optomechanical device where the exit slit of the spectrometer was replaced by a moving slit that repeatedly scanned the spectrum. The light passing the slit was recorded by a photomultiplier tube.

In the improved version of the instrument, a linear photodiode array detector is used. A schematic view of the absorption spectrometer is shown in Fig. 1.

The light source consists of a frequency doubled picosecond dye laser, synchronously pumped by a modelocked argon ion laser (Spectra Physics picosecond laser system). The separated ultraviolet light ($\lambda \simeq 308$ nm) had a bandwidth of about 0.15 nm, roughly a factor of 100 wider than the absorption linewidth of OH radicals. The laser beam is expanded to a diameter of 30 cm in order to reduce its divergence and to keep the level of self-generated OH radicals well below the detection limit. The beam is reflected back to the laboratory by a plane reflector 2.9 km away, so the total lightpath length is 5.8 km. The received laser light is focused onto the entrance slit of a high resolution double spectrometer (SPEX 1402, gratings 2160 lines/mm, blaze wavelength 500 nm, linear dispersion in second order 0.13 nm/mm).

The spectrum is recorded by a self-scanning linear photodiode array (Reticon RL 1024 S) and transferred to a microcomputer (DEC PDP 11/73) for signal averaging and further data evaluation. In order to adapt the dispersion of the spectrometer to the physical dimensions of the detector, it is necessary to magnify the spectrum about ten-fold (Fig. 2).

We obtained a scanning range of approximately 0.3 nm, which is covered by a row of 1024 light sensitive elements. The resolution of the spectrometer of 1.7 pm thus corresponds to at least 5 array elements.

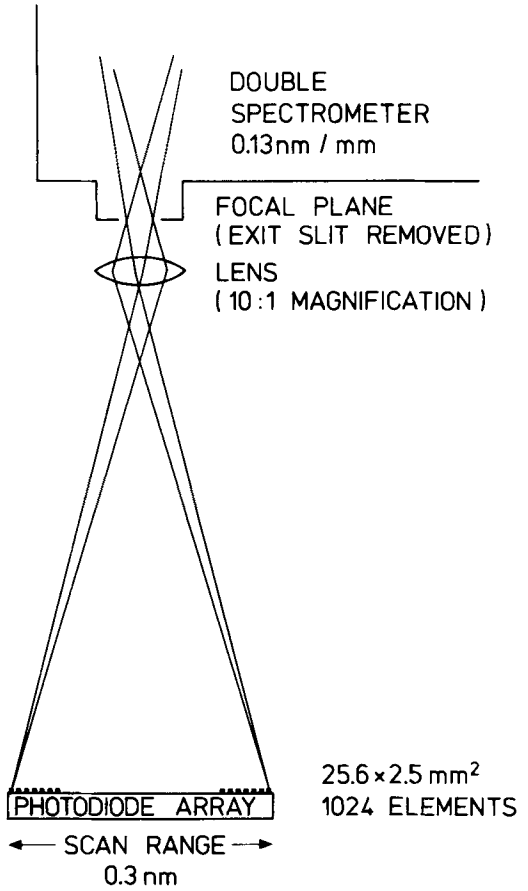

Fig. 2. Optical setup for enlarged imaging of the spectrum in the exit plane of the spectrometer onto the photodiode array.

Using this optoelectronic imaging device the following improvements were achieved:

- the spectral resolution is enhanced by about 30%;
- the scanning range could be extended 6-fold (from 0.05 nm to 0.3 nm); with an optomechanical detector this would only be possible at the expense of a decrease in duty cycle (scanning time for one spectral interval versus total integration time);
- in contrast to the optomechanical version the semiconductor device simultaneously records the entire spectral window of the spectrometer; the effective light utilization leads to a substantial reduction in measurement time.

Disadvantages of diode array spectrometers are the non-uniform response of the individual light sensitive diodes and the temperature dependent dark current.

The latter can be suppressed by cooling the detector to sufficiently low temperatures ($\leqslant$210K). The former must be eliminated by dividing the recorded air spectrum that carries the absorption structures by a laser spectrum without absorption features. This 'zero-spectrum' only contains information about the sensitivity of the individual diodes and can be obtained in different ways. We simply opened the entrance slit of the spectrometer to deteriorate the resolution of the instrument.

2.2. Noise sources and detection limit

The *detection limit* of the instrument is determined by the noise in the spectrum. There are 3 major sources of noise that have to be considered. The photoelectron noise (shot noise) of the detector, the temperature dependent dark current noise, and electronic noise sources. Earlier studies (Talmi and Simpson, 1980) have shown, that the dark current noise can be neglected at low detector temperatures.

Because we found the electronic noise of the commercially available systems to greatly exceed the shot noise level (Talmi, 1982), we were compelled to develop a special low-noise electronics for controlling and reading out the detector information. Our measurements showed that we succeeded to reduce the remaining electronic noise even below the shot noise level (Callies, 1985).

The fundamental limit of the detection sensitivity of a diode array detector is—in the absence of all other noise sources—determined by the generation of photoelectrons in the detector (shot noise), which follows the rules of Poisson statistics. Consequently, the actual detection limit is a function of the accumulated charge in the diode array elements and improves only with the square root of the amount of charge integrated.

In the case of our diode array, the peak-to-peak noise (difference between the maximum and minimum diode signals divided by the average signal level) in a 1024-channel quotient-spectrum (single readout, divided by a single readout zero-spectrum) at maximum possible signal level is calculated to be $\simeq 1.1 \cdot 10^{-3}$ according to the Poisson statistics. Together with the measured intensity independent noise of our electronics this

results in a value of $1.3 \cdot 10^{-3}$ for a single measurement. Because of this constant noise contribution, it is desirable to operate the detector close to the upper level of its dynamic range (close to the saturation level). However, the maximum signal level that effectively can be reached during measurements in the atmosphere is limited. Fluctuations of the received light intensity due to air movements easily can lead to an overload of the detector. Depending on the ambient conditions, the average charge accumulated in the detector during the integration time (measurement time for one spectrum) sometimes has to be reduced to about 30% of the saturation value. Under those conditions the resulting noise levels are $1.9 \cdot 10^{-3}$ and $2.3 \cdot 10^{-3}$, respectively.

In the laboratory using a Xe-arc as a light source and the same conditions as above, we actually achieved these values. Thus, due to the electronic contribution, the detection system is—within 20%—shot noise limited.

The noise limits discussed above describe the largest amplitude found in the spectrum, disregarding the shape of this structure. Computer simulations, however, showed that detectable absorption bands only correspond to about 50% of the peak-to-peak noise. Furthermore, the width of the narrowest *absorption* line in the spectrum is limited by the spectrometer to about 5 array elements. Thus, noise peaks with 'higher frequency' can be filtered out by mathematical methods reducing the remaining noise to levels of $\leqslant 1 \cdot 10^{-3}$ in a single measurement at 30% saturation.

Due to its statistical nature, the noise can be further reduced by superimposing consecutive readouts of the diode array. Averaging, for instance, 100 readouts, noise levels of $\simeq 1 \cdot 10^{-4}$ were achieved.

In contrast to the laboratory, spectra measured under atmospheric conditions show about 50% higher values. Typically $1.5 \cdot 10^{-4}$ were reached integrating over 100 readouts at an overall measurement time of 30 min (including the time needed to aquire zero spectra). We found that in several cases additional absorption lines were recorded in the spectra. Some of those always show up at the same wavelength positions, but at greatly varying strengths, other lines varied in both, strength and position. While the former are probably due to absorption by (yet unknown) atmospheric species, the latter are likely artefacts of the spectrometer system. Up to now, the reason for those apparent lines could not be definitely clarified. We have, however, experimental indications that air turbulence could cause varying illumination of the entrance slit of the spectrometer and therefore of the diffraction gratings and the elements of the photodiode array. Because individual diodes may have a non-uniform width over their length of 2.5 mm, illumination at different positions might lead to varying response characteristics ('optical noise').

Furthermore, the existence of presently unknown species absorbing in this wavelength range (as already described by Perner et al. (1987)) cannot be excluded.

Using Lambert-Beer's law, the detection limit of OH radicals according to the discussions above is about $2.4 \cdot 10^6$ OH molecules/cm^3 at 30 min integration time and the given lightpath length of 5.8 km. Here, an apparent absorption cross section at the centre of the $Q_1(3)$ line of $1.1 \cdot 10^{-16}$ cm^2 was used in the calculation. It was derived taking into account the measured instrument function and line shape (spectral resolution) of our spectrometer, the effect of smoothing the data, and the Voigt-shape of the OH absorption line at atmospheric pressure.

3. OH absorption spectra and interfering trace gases

The large scanning range of the diode array spectrometer allowed us to observe different absorption transitions of the OH radical (Fig. 3, $Q_1(2)$ and $Q_{12}(2)$ lines at $\lambda \simeq 308.0$ nm and $Q_1(3)$, $Q_{12}(3)$, and $P_1(1)$ lines at $\lambda \simeq 308.16$ nm).

Unfortunately we could not observe both wavelength regions simultaneously in one measurement, because of the limited emission-bandwidth of the laser system. Thus, usually we centred the maximum of the laser emission at the position of one group of absorption lines (either $Q_1(2)$, $Q_{12}(2)$ or $Q_1(3)$, $Q_{12}(3)$, $P_1(1)$) and did not change the observation wavelength during a measurement day. In this paper we will restrict the presentation and discussion of our results to measurements of the longer wavelength transitions. A further detailed description and interpretation of all recorded OH spectra from this year will be given in a forthcoming publication.

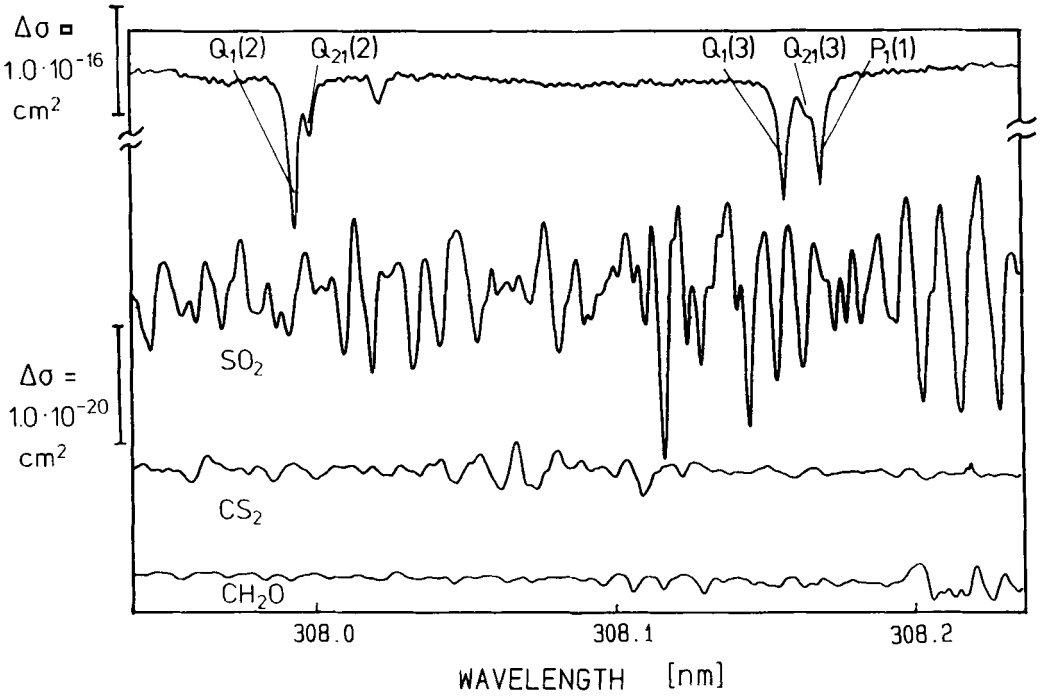

Fig. 3. Absorption spectra of OH radicals and some trace gases that interfere in OH measurements. The spectra were recorded in the laboratory using a Xe-arc light source. SO_2, CS_2, and HCHO were measured in quartz cuvettes, OH radicals were generated in a flow reactor of 1.14 m length, photolyzing a mixture of $O_2/O_3/H_2O$-vapor ($T = 298$ K, $p = 1.0$ bar) by four Hg low-pressure lamps (Philips TUV/40W).

The laboratory spectrum in Fig. 3 shows a section of an OH radical absorption spectrum. Under real measurement conditions in the troposphere this spectrum can be superimposed by absorption features of other trace gases.

In industralized regions, SO_2, for example, is roughly 10^5 times more abundant (typ. several ppb) than OH during daytime, while its absorption coefficient is only about 4 orders of magnitude lower. Thus, in polluted air, the atmospheric absorption spectra can be dominated by SO_2.

CS_2 and HCHO which also have absorption lines in this wavelength region are of minor influence because of their lower absorption coefficients and concentrations in ambient air.

In general, superimposed spectra can only be quantitatively (>99%) subtracted if the observed spectral interval contains enough significant information to unambiguously identify those absorption features. Fortunately, the measured wavelength interval has wide regions without OH absorption features (see Fig. 3) that are suited to identify absorptions of other trace gases.

4. Supporting measurements

Simultaneously to OH, we measured a set of parameters (see Table 1) that determine the actual OH concentration in ambient air, and therefore are essential as input parameters for model calculations.

The trace gases NO_2, SO_2, and HCHO were measured by their characteristic *vibrational* band structures, again using differential optical absorption spectroscopy (DOAS). This second spectrometer operates with a Xe-arc as a light source. Both LPA-instruments sampled the same air volume, and both used the same reflecting mirror. (For further details of the DOAS instrument see Platt et al., (1979), Platt and Perner (1983, 1984).

Table 1. *Most important parameters necessary for a characterization of the air mass and corresponding measurement technique*

SO_2	DOAS*
HCHO	DOAS
NO_2	DOAS, chemiluminescence
NO	chemiluminescence
O_3	UV-photometer (DASIBI)
CO	gas chromatography
CH_4	gas chromatography
hydrocarbons	gas chromatography
H_2O	psychrometer
$J(O_3)$	absolute calibrated photoelectric sensors
$J(NO_2)$	absolute calibrated photoelectric sensors
aerosol	nephelometer
temperature	standard meteorologic instrumentation using a computerized data recording system
air pressure	standard meteorologic instrumentation using a computerized data recording system
wind speed	standard meteorologic instrumentation using a computerized data recording system
wind direction	standard meteorologic instrumentation using a computerized data recording system

* DOAS = differential optical absorption spectroscopy.

5. Results and data evaluation

An example of an atmospheric absorption spectrum is presented in Fig. 4. It is part of a spectrum recorded with the diode array detector on July 14, 1987 in Jülich.

Jülich is a relatively polluted site; therefore, the air spectrum shows a strong SO_2 absorption structure. For comparison, the second spectrum is that of pure SO_2.

The lowest trace in Fig. 4 shows the residual air spectrum after subtraction of the SO_2 absorptions. OH radical absorption bands, that are already marginally indicated in spectrum 1 (arrows), can be recognized at the position given by the OH reference spectrum. In addition some, up to now, not identified absorption features appear in the spectrum. These unknown bands showed irregular temporal variations in strength during the day, in contrast to the OH lines which gave a distinct diurnal profile. Unknown absorption features of varying strength at a number of wavelength positions were already observed during OH measurements in Jülich 1982 (see Perner et al. (1987)).

It is not an easy task to identify and quantify small OH absorption structures in a noisy spectrum, as is illustrated by Fig. 4. We developed the following procedure. First, the exact positions of the OH lines are determined using a laboratory source of OH radicals and measuring its spectrum before and after recording air spectra. Second, the region around the absorption bands of this OH reference spectrum is fitted to the air spectrum and the minimum mean square sum of deviation, χ^2, is calculated. Third, the reference spectrum is shifted from the correct wavelength position in small steps left and right and the corresponding χ^2 is calculated. The resulting plot of χ^2 against the shift in wavelength shows a

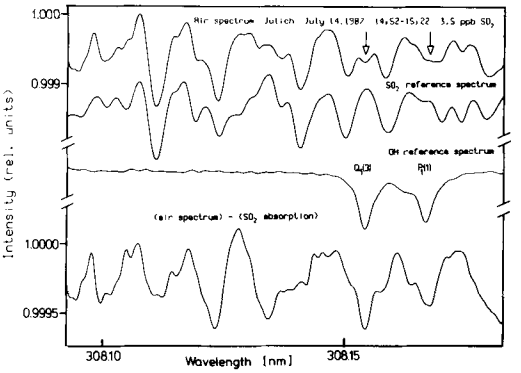

Fig. 4. 1st trace: Air spectrum recorded in Jülich, integrated over 100 measurements during 30 min. *2nd trace*: Absorption spectrum of pure SO_2 (quartz cuvette filled with SO_2). *3rd trace*: Absorption spectrum of OH radicals ($T = 298$ K, $p = 1.0$ bar). *4th trace*: Residual air spectrum after subtraction of SO_2 absorption.

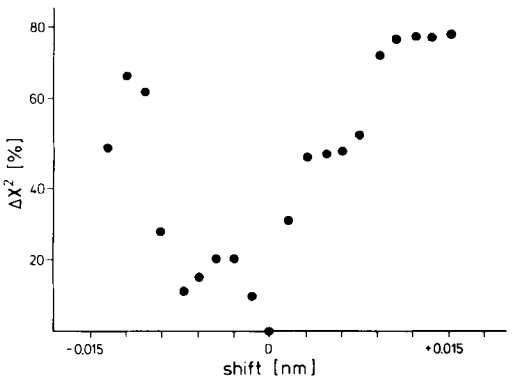

Fig. 5. Deviation of the mean square error sum $\Delta\chi^2 = \chi^2(\Delta\lambda) - \chi^2(\Delta\lambda = 0)$ of a fit of the OH reference spectrum to the residual air spectrum in Fig. 4 as a function of the wavelength shift $\Delta\lambda$ of the OH reference spectrum.

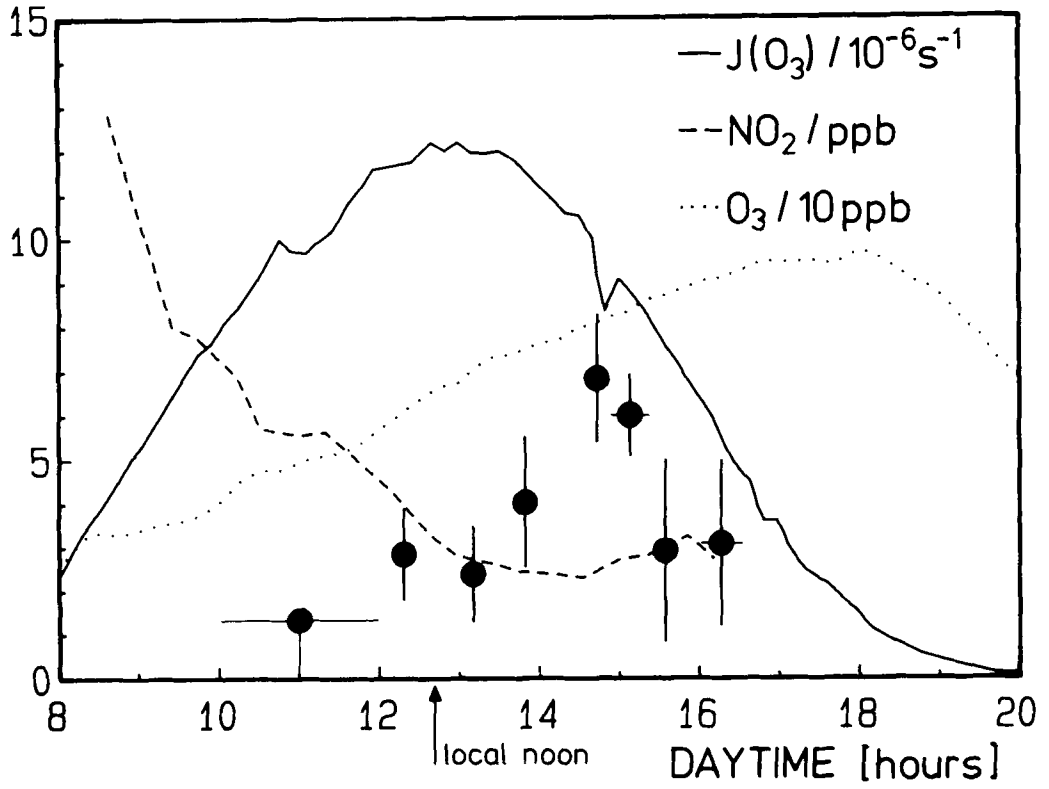

Fig. 6. Diurnal profile of the OH concentration (filled circles, scale: 10^6 cm^{-3}), O_3 photolysis frequency, $J(O_3)$, (drawn line), NO_2 mixing ratio (dashed line), and O_3 mixing ratio (dotted line) in Jülich on 14 July, 1987. Horizontal bars indicate integration times, vertical bars the 1σ errors of the OH concentration. The data point in the morning corresponds to the upper limit of the OH concentration (see text).

minimum at the shift zero, when OH is present (see Fig. 5).

Finally, the actual OH radical concentration is calculated from the scaled OH reference spectrum fitted at zero shift. The 1σ error is estimated from the measured spectrum taking all apparent absorption features as random noise.

The diurnal profile of the OH concentration obtained on July 14, 1987 is plotted in Fig. 6 together with the profiles of NO_2, O_3, and ozone photolysis frequency, $J(O_3)$.

A summary of the gas chromatographic analysis of an air sample is given in Table 2. Diurnal profiles of HCHO, SO_2, $J(NO_2)$, and the aerosol light scattering signal, β, (corresponding to the effective aerosol surface per unit volume) are plotted in Fig. 7. Additionally, chemiluminescence measurements of NO are shown.

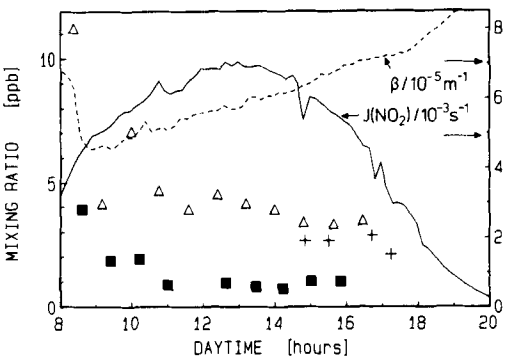

Fig. 7. Diurnal profiles of SO_2 (triangles), HCHO (squares), NO_2 photolysis frequency, $J(NO_2)$ (drawn line, right scale), and aerosol light scattering signal, β (dashed line, right scale) on 14 July 1987. Mixing ratios of NO (crosses, values multiplied by 10) measured by chemiluminescence are added for completeness.

Table 2. *Gas chromatographic analysis of the air sample taken on July 14, 1987 1:40 pm (mixing ratios in ppb)*

methane	1705.00	CO	189.00	
ethane	1.65	ethene	0.55	ethine 0.58
propane	1.08	propene	0.66	
n-butane	0.72	1-butene	0.90	
i-butane	0.22			
methylchloride	0.54			

Note, that the calculated NO/NO_2 ratios in the $NO/NO_2/O_3$ system alone are about 50% higher than the observed values.

6. Discussion

Comparison of the diurnal profile of OH with that of $J(O_3)$ (which is a measure for the primary production of tropospheric OH radicals) shows, that the increase of the OH concentration is delayed with respect to the rise of $J(O_3)$. The peak value in OH appears roughly two hours after local noon, 1 h after the maximum $J(O_3)$ was reached. Between 10:00 am and 12:00 pm no absorption bands could be determined in the spectra, so only an upper limit (sum of signal and 1σ error) is given.

A look at the profile of the NO_2 concentration offers an explanation of this asymmetric profile. During the morning hours, NO_2 concentrations higher than 10 ppb were present. At NO_2 concentrations of a few ppb, the reaction of OH with NO_2 forming nitric acid (HNO_3) is the major and irreversible sink for OH radicals. Therefore, the OH concentration remained below the detection limit as long as the NO_2 concentration was above ≈ 5 ppb.

The continued decrease in the NO_2 concentration at noon to values below 4 ppb eventually allowed an increase of OH radicals, because the destruction reaction is slowed down, while the primary production of OH is even stronger due to the increasing ozone concentration at nearly constant photolysis frequency. In the later afternoon (at low NO_2) the decay of the OH concentration is governed by the decrease of the primary source process.

A very simple estimate supports this qualitative interpretation. Considering only the primary formation reaction of OH radicals (ozone photolysis (1) and reaction of the $O(^1D)$ atoms with water vapor (4); all rate constants in units of cm^3/molec·s and evaluated for 298°K, 1 bar)

$$O_3 + h\nu \text{ ---> } O(^1D) + O_2 \quad J(O_3) \tag{1}$$

$$O(^1D) + O_2 \text{ ---> } O(^3P) + O_2 \quad k_2 = 4.0 \cdot 10^{-11} \tag{2}$$

$$+ N_2 \text{ ---> } O(^3P) + N_2 \quad k_3 = 2.6 \cdot 10^{-11} \tag{3}$$

$$+ H_2O \text{ ---> } 2\,OH \quad k_4 = 2.2 \cdot 10^{-10} \tag{4}$$

and the irreversible destruction reaction

$$OH + NO_2 \text{ -M-> } HNO_3 \quad k_5 = 1.16 \cdot 10^{-11} \tag{5}$$

one can calculate the stationary OH concentration from

$$[OH]_{stat} = 2k_4[H_2O][O(^1D)]_{stat}/(k_5[NO_2]),$$

with

$$[O(^1D)]_{stat} = J(O_3)[O_3]/(k_2[O_2] + k_3[N_2] + k_4[H_2O]).$$

The so estimated OH concentrations are given in Table 3. The values show the same trend as the experimental observations.

7. Conclusion

We demonstrated the usefulness of a diode array detector for the measurement of tropospheric hydroxyl radical concentrations in polluted air. The large spectral range covered by this device simplifies and improves the measurement technique considerably. The broadband excitation and detection technique allows more reliable identification of interferences and the measurement times become shorter.

We have shown the importance of supporting measurements performed during the time of OH measurements. Only a sufficiently complete chemical characterization of the air mass can provide the basis for meaningful model calculations to interprete the measured OH concentration profiles.

Further improvements of the experimental setup are necessary. We are presently changing the optical system in order to broaden the second harmonic bandwidth of the laser and to reduce

Table 3. *Estimate of the stationary OH concentration in Jülich, 14 July 1987*

Time of day local time	NO_2 (ppb)	O_3 (ppb)	$J(O_3)$ (s^{-1})	H_2O (10^{17} cm^{-3})	$[OH]_{stat}$ (cm^{-3})
11:00	5.6	49	$0.96 \cdot 10^{-5}$	3.35	$1.3 \cdot 10^6$
12:00	4.6	57	$1.17 \cdot 10^{-5}$	3.42	$2.4 \cdot 10^6$
13:00	2.9	68	$1.21 \cdot 10^{-5}$	3.45	$4.7 \cdot 10^6$
14:00	2.4	76	$1.11 \cdot 10^{-5}$	3.50	$5.9 \cdot 10^6$
15:00	2.7	83	$0.91 \cdot 10^{-5}$	3.50	$4.7 \cdot 10^6$
16:00	3.1	90	$0.64 \cdot 10^{-5}$	3.40	$3.0 \cdot 10^6$

the influence of air turbulences ('optical noise'). Furthermore, we are trying to identify other atmospheric species that have absorption lines in the observed spectral region and might appear in sufficient concentration in ambient air to interfere with OH measurements.

8. Acknowledgement

We thank Dr. J. Rudolph and coworkers for measuring hydrocarbons by gas chromatography and Dr. F. Rohrer and D. Brüning for measuring NO and NO_2 by chemiluminescence.

REFERENCES

Callies, J. 1985. Test of a photodiode array for measurements of atmospheric trace gases by absorption spectroscopy (in German). Diploma thesis, University of Bonn and Kernforschungsanlage Jülich, FRG.

Campbell, M. J., Farmer, J. C., Fitzner, C. A., Henry, M. N., Sheppard, J. C., Hardy, R. J., Hopper, J. and Muralidhar, V. 1986. Radiocarbon tracer measurements of atmospheric hydroxyl radical concentrations. *J. Atmos. Chem. 4*, 413–428.

Davis, L. I. Jr., James, J. V., Wang, C. C., Guo, C., Morris, P. T. and Fishman, J. 1987. OH measurement near the intertropical convergence zone in the pacific. *J. Geophys. Res. D92*, 2020–2024.

Ehhalt, D. H. 1974. The atmospheric cycle of methane. *Tellus* 26, 58–70.

Ehhalt, D. H. 1987. Free radicals in the atmosphere. *Free Rad. Res. Comms. 3*, 153–164.

Hard, T. M., Chan, C. Y., Mehrabzadeh, A. A., Pan, W. H. and O'Brian, R. J. 1986. Diurnal cycle of tropospheric HO. *Nature 322*, 617–620.

Hewitt, C. N. and Harrison, R. M. 1985. Tropospheric concentrations of the hydroxyl radical—a review. *Atmos. Environ. 19*, 545–554.

Hübler, G., Perner, D., Platt, U., Tönnissen, A. and Ehhalt, D. H. 1984. Groundlevel OH Radical Concentration: New Measurements by Optical Absorption. *J. Geophys. Res. 89*, 1309–1319.

Perner, D., Platt, U., Trainer, M., Hübler, G., Drummond, J. W., Junkermann, W., Rudolph, J., Schubert, B., Volz, A., Ehhalt, D. H., Rumpel, K. J. and Helas, G. 1987. Tropospheric OH concentrations: A comparison of field data with model predictions. *J. Atmosph. Chem. 5*, 185–216.

Platt, U., Perner, D. and Pätz, H. 1979. Simultaneous measurement of atmospheric HCHO, O_3, and NO_2 by differential optical absorption. *J. Geophys. Res. 84*, 6329–6335.

Platt, U. and Perner, D. 1983. Measurements of atmospheric trace gases by long path differential UV/visible absorption spectroscopy. In *Springer Ser. Opt. Sci. 39, Optical and Laser Remote Sensing* (ed. D. K. Killinger and A. Mooradian). Heidelberg: Springer, 95–105.

Platt, U. and Perner, D. 1984. An instrument for spectroscopic trace gas measurements in the atmosphere (in German). *Fresenius Z. Anal. Chem. 317*, 309–313.

Platt, U., Rateike, M., Junkermann, W., Hofzumahaus, A. and Ehhalt, D. H. 1987. Detection of atmospheric OH radicals. *Free Rad. Res. Comms. 3*, 165–172.

Shirinzadeh, B., Wang, C. C. and Deng, D. Q. 1987. Diurnal variation of the OH concentration in ambient air. *Geophys. Res. Lett. 14*, 123–126.

Talmi, Y. and Simpson, R. W. 1980. Self-scanned photodiode array: a multichannel spectrometric detector. *Applied Optics 19*, 1401–1414.

Talmi, Y. 1982. Spectrophotometry and spectrofluorometry with the self-scanned photodiode array. *Appl. Spectrosc. 36*, 1–18.

Volz, A., Ehhalt, D. H. and Derwent, R. G. 1981. Seasonal and latitudinal variation of ^{14}CO and the tropospheric concentration of OH radicals. *J. Geophys. Res. 86*, 5163–5171.

Zimmermann, P. R., Chatfield, R. B., Fishman, J., Crutzen, P. J. and Hanst, P. L. 1978. Estimates on the production of CO and H_2 from the oxidation of hydrocarbon emissions from vegetation. *Geophys. Res. Lett. 5*, 679–682.